

# The molecular Zeeman effect and diagnostics of solar and stellar magnetic fields

## II. Synthetic Stokes profiles in the Zeeman regime

S. V. Berdyugina<sup>1,2</sup>, S. K. Solanki<sup>3</sup>, and C. Frutiger<sup>1</sup>

<sup>1</sup> Institut für Astronomie, ETH, 8092 Zürich, Switzerland

<sup>2</sup> Astronomy Division, PO Box 3000, 90014 University of Oulu, Finland

<sup>3</sup> Max-Planck-Institut für Aeronomie, 37191 Katlenburg-Lindau, Germany

Received 28 April 2003 / Accepted 4 September 2003

**Abstract.** Recent advances in the computation of the Zeeman splitting of molecular lines have paved the way for their use as diagnostics of solar and stellar magnetic fields. A systematic study of their diagnostic capabilities had not been carried out so far, however. Here we investigate how molecular lines can be used to deduce the magnetic and thermal structure of sunspots, starspots and cool stars. First, we briefly describe the Stokes radiative transfer of Zeeman-split molecular lines. Then, we compute Stokes spectra of TiO, OH, CH and FeH lines and investigate their diagnostic capabilities. We also compare the synthetic profiles with observations. Spectra of TiO, OH and FeH are found to be interesting diagnostics of sunspot magnetic fields. This is also true for cool stars, where, however, the OH Stokes  $V$  profiles may require very high S/N data to be reliably employed. Finally we investigate the potential of various molecular bands for high-contrast imaging of the solar surface. The violet CN and CH bands turn out to be most promising for imaging the photosphere, the TiO bands are excellent for imaging sunspot umbrae, while the UV OH band can be used for imaging both the photosphere and sunspots.

**Key words.** molecular processes – Sun: magnetic fields – stars: magnetic fields – techniques: polarimetric

### 1. Introduction

The spectra of sunspots and of cool stars contain a rich collection of molecular lines (e.g. Wallace et al. 1998). Lines of diatomic molecules observed in sunspot spectra are good temperature and pressure indicators. They are also useful for determining elemental and isotopic abundances. Recently we performed an overview of the magnetic properties of molecular band systems observed in visible and near infrared spectra of sunspots and cool stars. We showed that many molecular lines are also good indicators of solar and stellar magnetic fields (Berdyugina et al. 2000; Berdyugina & Solanki 2002, hereafter Paper I).

The use of molecular lines for studying the structure of sunspots brings real gains. One is the extension of sunspot models, including the magnetic field, to layers, where atomic lines suffer from NLTE effects, but molecules constituted of atoms that are predominantly neutral can be treated in LTE (cf. Johnson 1994). Simultaneous inversions of Stokes profiles of atomic and molecular lines observed in spectra of umbrae and penumbrae can thus potentially improve the current models of sunspots quite significantly. For example, the diagnostic

capabilities of the 1.56  $\mu\text{m}$  lines of Fe I are strongly compromised in umbrae due to their limited temperature sensitivity. By employing simultaneously measured OH lines, however, this shortcoming can be overcome (Mathew et al. 2003). Also, since molecular lines are extremely temperature sensitive they can be used to probe the thermal and magnetic structure of the coolest parts of sunspots at field strengths of 2–3.5 kG. Furthermore, in cool umbrae many atomic lines are heavily blended by molecular transitions. In order to obtain reliable information in these cases the molecular lines need to be computed along with the atomic transitions.

On cool stars with magnetic activity, such as T Tauri stars, solar type G-K dwarfs, RS CVn- and FK Com-type stars, molecular lines can provide measurements of magnetic fields directly in spatially unresolved spots, wherein they are formed (Berdyugina 2002). Atomic lines are of only very limited use in this case, since they obtain a strong contribution from outside the starspots, which completely swamps the weak signal from the starspots. The signal is weak due to the small spot filling factor (typically 10–20% as deduced from Doppler images, cf. Berdyugina et al. 1999, 2000) and the low continuum intensity in umbrae (typically 10–20% that of the unperturbed photosphere). Many molecular lines are vastly stronger in starspot umbrae, so that the observed line profile provides

relatively clean information on the physical characteristics of the starspots. Also, since molecular lines dominate spectra of cool dMe stars and brown dwarfs, their magnetic fields can be measured only by means of the molecular Zeeman effect (e.g. Valenti et al. 2001). This will help in understanding how strong the magnetic fields in fully convective stars can be.

Here we discuss a sample of molecular bands and lines which provide interesting diagnostics of stellar and solar magnetic features. Using the theoretical Zeeman patterns calculated as described in Paper I, we carried out the forward spectral synthesis of Stokes parameters of molecular transitions of interest. In Sect. 2, we formulate the polarized radiative transfer problem for molecular lines in the presence of a magnetic field and discuss an extended and improved version of the code STOPRO (Solanki et al. 1992; Frutiger et al. 2000), which solves the set of radiative transfer equations. We describe how the code was updated to enable computations of the molecular line absorption coefficient, the wavelength shifts and theoretical strengths of the Zeeman components and molecular number densities. In Sect. 3, we present calculations of polarization patterns of lines of diatomic molecules in the Zeeman regime and explore the opportunities for diagnosis of weak and moderate stellar and solar magnetic fields with molecular lines. The expression “weak and moderate magnetic fields” is to be understood in the sense that we only consider the Zeeman effect and, as in Paper I, do not deal with magnetic fields of sufficient strength to produce the Paschen-Back effect. The numerical value of the field strength beyond which the Zeeman regime is no longer valid depends on the molecular band in question. Rough estimates of this critical field strength are listed in Table 1 of Paper I for molecules of interest for solar and stellar studies. In Sect. 4, we investigate the sensitivity of the discussed molecules to the thermal structure of the solar/stellar atmosphere. Finally, we present our conclusions in Sect. 5.

## 2. Synthesis of molecular Stokes parameters

### 2.1. The radiative transfer equation

Here we describe the forward spectral synthesis of the Stokes parameters of molecular transitions. This was implemented into the code STOPRO described by Solanki (1987) and Solanki et al. (1992), which was recently extended and improved by Frutiger et al. (2000).

The set of radiative transfer equations is solved using the formulation given by Rees et al. (1989). The transfer equation for the Stokes vector is

$$\frac{d\mathbf{I}}{dz} = -\mathbf{K}\mathbf{I} + \mathbf{j}, \quad (1)$$

where  $\mathbf{K}$  is the total absorption matrix,

$$\mathbf{K} = k_c \mathbf{1} + k_0 \Phi, \quad (2)$$

and  $\mathbf{j}$  is the total emission vector,

$$\mathbf{j} = k_c S_c \mathbf{e}_0 + k_0 S_1 \Phi \mathbf{e}_0. \quad (3)$$

Here  $\mathbf{1}$  is the unit  $4 \times 4$  matrix,  $\mathbf{e}_0 = (1, 0, 0, 0)^T$ .  $k_c$  and  $S_c$  are the opacity and source function in the unpolarized continuum.

We assume Local Thermodynamic Equilibrium (LTE) and set  $S_c = B_\nu(T)$ , the Planck function at the local temperature  $T$ . The line centre opacity  $k_0$  is calculated for zero damping and zero magnetic field (see Sect. 2.2). The line source function  $S_1$  is also assumed to be determined by the local temperature, i.e.  $S_1 = S_c$ . The line absorption matrix  $\Phi$  is expressed via generalized absorption and anomalous dispersion profiles (see Rees et al. 1989). It is identical for atomic and molecular transitions once the splitting pattern of the spectral line is prescribed, e.g., following the theory presented in Paper I.

### 2.2. Absorption in molecular lines

The molecular line centre absorption coefficient is calculated as follows:

$$k_0 = \frac{\sqrt{\pi} e^2}{m_e c^2} \frac{\lambda_{J'J''}^2}{\Delta\lambda_D} f_{J'J''} \mathcal{N} \frac{2J'' + 1}{Q} e^{-E_{J''} \frac{hc}{kT}}, \quad (4)$$

where  $f_{J'J''}$  is the absorption oscillator strength,  $\mathcal{N}$  is the number density of a given molecule,  $Q$  its partition function,  $J'$  and  $J''$  indicate the upper and lower level involved in the transition,  $\lambda_{J'J''}$  is the wavelength of the transition,  $\Delta\lambda_D$  is the Doppler width, and  $E_{J''}$  is the lower level excitation energy. The symbols  $e$ ,  $m_e$ ,  $c$ ,  $h$  and  $k$  have their usual meaning. The absorption coefficient is also corrected for stimulated emission.

The absorption oscillator strength  $f_{J'J''}$  is related to the Hönl-London factor  $S_{J'J''}$  as follows (Schadee 1967):

$$f_{J'J''} = f_{\nu'\nu''} \frac{S_{J'J''}}{2J'' + 1} \frac{\lambda_{\nu'\nu''}}{\lambda_{J'J''}}. \quad (5)$$

The Hönl-London factor represents the full theoretical strength of the molecular line. It is different for different coupling cases (Hund’s cases) and was discussed in Paper I.  $f_{\nu'\nu''}$  and  $\lambda_{\nu'\nu''}$  are the oscillator strength and wavelength of the vibrational band ( $\nu'$ ,  $\nu''$ ) within which the rotational transition occurs. These are taken from laboratory measurements.

In order to account for blends, contributions from absorption and anomalous dispersion profiles in molecular and atomic lines are summed at each wavelength of the synthetic spectrum. Then, the radiative transfer Eq. (1) is solved.

### 2.3. Chemical equilibrium calculations

Molecular number densities are calculated under the assumption of chemical equilibrium between the different atomic and molecular species. In cool stellar atmospheres, two equilibrium processes are important: ionization and dissociation (e.g. Tsuji 1973). The first is computed employing the Saha equation, for the second we make the assumption of chemical equilibrium, i.e., the number of associations equals the number of dissociations:

$$A + B \leftrightarrow AB. \quad (6)$$

Then, the ratio of number densities of species involved in the reaction is expressed via the equilibrium constants  $K'_{AB}$ :

$$\frac{N(A)N(B)}{N(AB)} = K'_{AB}(T),$$

$$K'_{AB}(T) = \left( \frac{2\pi m_{AB}kT}{h^2} \right)^{\frac{3}{2}} \frac{Q_A Q_B}{Q_{AB}} \exp\left(-\frac{D_0}{kT}\right). \quad (7)$$

According to Eq. (7)  $K'_{AB}(T)$  depends primarily on the local temperature  $T$ , the dissociation potential of the molecule  $D_0$ , the molecular mass  $m_{AB}$ , and atomic and molecular partition functions  $Q_A, Q_B, Q_{AB}$ .

The total number of atoms of a given element  $X_i$  is the sum of free atoms and atoms coupled in molecules:

$$n(X_i) = N(X_i) + 2N(X_iX_i) + \sum_j N(X_iX_j). \quad (8)$$

To the system of such equations for a number of elements, two more equations are added. The first is the equation of charge conservation, which is imposed through the electron number density,

$$n_e = \sum_i \sum_l lN_{il}, \quad (9)$$

where  $N_{il}$  is the number of ions in ionization state  $l$  of element  $X_i$  and  $n_e$  is the number density of electrons. The second additional equation describes particle number conservation:

$$\mathcal{P}_g = \left( \sum_i N_i^0 + \sum_i \sum_l N_{il} + n_e + N_{\text{mol}} \right) kT, \quad (10)$$

where  $N_{\text{mol}}$  is the number of molecules. Given a model stellar atmosphere, the system of nonlinear equations is solved with the Newton-Raphson method for 270 compounds consisting of the 33 most abundant atoms (Tsuji 1973; L. Hänni, private communication). The equilibrium constants tabulated by Tsuji (1973) as polynomials were corrected for new values of the dissociation energies. This is important since molecular number densities are strongly sensitive to the dissociation potential, as seen from Eq. (7).

#### 2.4. The validity of the equilibrium assumptions

The assumption of LTE for the line source function is fulfilled to a high degree for molecular species in solar and stellar atmospheres (cf. Johnson 1994). Departures from LTE in level populations can occur, however, if radiative rates exceed collisional rates of transitions. For instance, energies of molecular electronic transitions may exceed the average kinetic energy of particles and, thus, such transitions can be significantly affected by NLTE effects, especially in the outer layers of cool stellar atmospheres. In the outer solar atmosphere, above the temperature-minimum region, departures from LTE in molecular electronic transitions were predicted in CH and CO as overpopulation of levels relative to LTE (Anderson 1989). Energies of ro-vibrational and pure rotational transitions are comparable or smaller than the kinetic energy of colliding particles and, thus, vibrational and rotational levels are likely to be in LTE

in the solar atmosphere. This was confirmed, for instance, by a careful NLTE calculation of CO by Ayres & Wiedemann (1989).

The most significant NLTE effect on molecular opacities could arise from overionization of neutral atoms, which might reduce the pool from which molecules can be made. This effect will not occur for molecules composed of the abundant elements H, C, N, and O because of their large ionization energies (11–15 eV). However, molecules containing, e.g., Fe, Ti, Mg might be affected by overionization, as the ionization energies of these atoms are lower, in the range 7–8 eV. As discussed by Rutten (1988), however, conclusions about the absence or presence of overionization or NLTE effects in photospheric lines depend strongly on the model atmosphere employed, with models deduced assuming LTE giving rise to smaller NLTE effects. Thus, the question of overionization is not as yet completely resolved, although the problem is less severe than believed earlier.

### 3. Magnetic molecular diagnostics

Here we discuss those electronic systems of the molecules presented in Paper I that can be treated in the Zeeman regime for typical strengths of solar and (non-degenerate) stellar photospheric magnetic fields, i.e. for fields between 500 G and 5000 G. Other molecules whose band systems are formed in the Paschen-Back regime at such weak fields will be considered in a forthcoming paper. In Paper I we looked for strong lines with as little blending as possible and a high enough magnetic sensitivity, so that they can be used to diagnose surface magnetic fields in the Sun and other stars. The conclusions reached in Paper I indicate therefore the lines of first choice – those with the largest effective Landé factors (see Table 1)<sup>1</sup>. Among those, the strongest and least blended are lines belonging to the TiO (0,0) band of the  $\gamma$ -system, OH ro-vibrational infrared lines and the FeH (0,0) band of the  $F - X$  system. Below we present calculations of the Stokes parameters for these bands and compare them, where possible, with observations in sunspots. We also compute the CH A-X system bands at 4310 Å since these have been used for imaging of small-scale magnetic fields in the solar photosphere and it is interesting to determine the Stokes  $V$  signal associated with these bands.

These lines have also been detected in the spectra of magnetically active stars of spectral type G and later. Since many of these stars are too hot to give rise to TiO or FeH spectra in their unperturbed photospheres, these lines are interpreted to form in starspots, i.e. cool magnetic inhomogeneities on the surfaces of active stars (e.g., Ramsey & Nations 1980). We therefore estimate the possibility for the polarization due to the Zeeman effect to be detected in these lines from starspots, under the commonly made assumption that they are magnetic. Zeeman

<sup>1</sup> As kindly pointed out by E. Landi Degl'Innocenti the *effective* Landé factors given and plotted in Paper I are all too large by a factor of 2. They, in fact, represent the average splitting in units of the normal Zeeman splitting. In the present paper, e.g. in Table 1, we provide corrected values. Note that effective Landé factors were not used for Stokes profile calculations

**Table 1.** Diatomic molecules having transitions in the optical and near IR that can be treated in the Zeeman regime for typical solar and stellar photospheric magnetic field strengths. Here,  $g_{\text{eff}}$  is the maximum effective Landé factor in a given band system.

System	Max $g_{\text{eff}}$	Branch of max $g_{\text{eff}}$	$\lambda$ (band)	
			of max $g_{\text{eff}}$	
TiO	$\gamma : A^3\Phi - X^3\Delta$	+1.1	$R_3$	7054 (0,0)
	$\gamma' : B^3\Pi - X^3\Delta$	+1.1	$P_3$	6224 (0,0)
	$\alpha : C^3\Delta - X^3\Delta$	+1.0	$Q_3$	weak
	$\delta : b^1\Pi - a^1\Delta$	+1.2	$P$	8860 (0,0)
	$\beta : c^1\Phi - a^1\Delta$	+1.4	$R$	5597 (0,0)
OH	$X^2\Pi$	$\pm 0.16$	$P_1, P_2$	14 882 (2,0)
				15 328 (3,1)
				16 124 (4,2)
FeH	$F^4\Delta - X^4\Delta$	+1.1	$Q_{7/2}$	10 062 (0,0)
CH	$A^2\Delta - X^2\Pi$	+1.0	$R_1$	4300 (0,0)
$C_2$	$d^3\Pi - a^3\Pi$	$\pm 0.3$	$P_1, P_3$	5165 (0,0)

polarization from atomic lines is not seen to emerge from the dark cores of starspots (Donati et al. 1999).

### 3.1. TiO

TiO lines are prominent in spectra of sunspots and cool stars. The first astronomical detection of TiO lines was in spectra of M-type stars (Fowler 1904) where they dominate the visible and near-infrared spectrum. The identification of the TiO  $\alpha$ - and  $\gamma$ -system bands in sunspots dates back to the early part of the 20th century by Hale et al. (1906) and Hale & Adams (1907), respectively. More recently, the  $\gamma'$  bands (Wöhl 1971),  $\beta$  bands (Sotirovski 1972) and  $\delta$  bands (Ram et al. 1996) have also been identified in sunspots. The rich TiO spectra were used to determine temperatures and Ti isotope abundances (cf. Lambert & Mallia 1972) as well as to obtain improved molecular constants (Ram et al. 1999). They have never been used for magnetic solar and stellar studies as yet.

The idea that TiO bands could be used to measure starspot properties was first stated by Ramsey & Nations (1980). They observed a TiO band in the spectrum of the active G5 IV + K1 IV system V711 Tau (HR1099) near its photometric minimum. The spectral classes of the binary components excluded the possibility for the band to be formed in the unspotted photosphere, so that the TiO feature must be produced in starspots that are at least 1000 K cooler than the photosphere of the K1 IV star. Further observations revealed TiO bands in the spectra of other active stars of sufficiently early spectral type, which allowed the spot area and temperature to be measured (e.g. Neff et al. 1995; O'Neal et al. 1996).

#### 3.1.1. The TiO $\gamma$ -system in sunspots

In sunspot umbrae, the (0,0) $R_3$  band head of the  $\gamma$ -system ( $A^3\Phi - X^3\Delta$ ) at 7054 Å is the strongest molecular absorption feature in the visible. Remarkably, lines of this system are also strongly magnetically sensitive, especially in the  $P_3$

and  $R_3$  branches, with effective Landé factors  $|g_{\text{eff}}| \leq 1.1$  (Paper I). The wavelength separation between rotational lines in the band is small and lines of low rotational numbers (larger splitting) almost coincide with those of high numbers (smaller splitting) in the band head. Thus each TiO line shortward of 7057 Å in Fig. 1 is actually a blend of (at least) two lines, one with high  $J$ , one with low  $J$ , so that the sum of  $J$ s is the same for all lines. Since the Landé factor decreases with  $J$ , this blending implies that the effective Landé factor of each pair of blends (appearing as a single line) changes much less than Fig. 6 of Paper I would suggest. As a result, a clear polarization signal appears in the band.

Recently, we presented the first Stokes  $V$  observation of the  $\gamma$  (0,0) $R_3$  band head in a sunspot (Berdyugina et al. 2000). We successfully reproduced it with our calculations, under the assumption that the electronic states of the  $\gamma$ -system are described by pure Hund's case (a), i.e. that spin is strongly coupled to the internuclear axis of the molecule. In Paper I we showed, however, that small perturbations due to spin uncoupling can be seen for higher rotational levels (Fig. 6 in Paper I). This results in a slight increase of the absolute values of the effective Landé factors of the  $P_1$ ,  $P_3$  and  $R_1$ ,  $R_3$  branches as rotational number increases. Here we perform a new calculation of the  $R_3$  (0,0) band head which takes into account the perturbation.

In Fig. 1 we present the observed Stokes  $I$  and  $V$  profiles compared with the new synthetic spectrum. Along with the TiO (0,0) $R_3$  lines, the employed line list includes a number of atomic lines and weak TiO lines from higher vibrational bands of the  $\gamma$ -system. Since the observations are affected by stray light from the photosphere, we combined calculated sunspot and photospheric spectra using a spot filling factor of 0.75 prior to plotting them. A significant improvement of the fit relative to that shown by Berdyugina et al. (2000) is seen in the  $R_3(30)$  and  $R_3(31)$  lines at 7057.2 Å and 7057.7 Å, as their effective Landé factors increased by a factor of approximately two. This provides strong support for the correctness of the perturbation analysis presented in Paper I.

The Stokes  $V$  observations are excellently reproduced. This suggests that our current understanding of molecular Zeeman splitting underlying such calculations is adequate for this band. The main contribution to the polarization is due to the TiO (0,0) $R_3$  lines. Other TiO lines, from higher vibrational bands and rotational levels, are not Zeeman sensitive. Stokes  $I$  however suggests that our spectral synthesis does not include all lines and that some of the blends are not identified (some are telluric lines). Nonetheless, we expect this band to be very useful for future investigations of cool magnetic structures in the solar photosphere, since Stokes  $V$  is the important quantity for deducing magnetic properties.

In order to study the magnetic sensitivity of lines in this band we carried out calculations of Stokes  $I$  and  $V$  profiles of one representative line, namely  $R_3(10)$  with an effective Landé factor of 0.4, at different magnetic field strengths. The result is shown in Fig. 2. It is seen that the line starts to become fully-split in Stokes  $V$  at about 2.5 kG and that Stokes  $V$  shows clear signs of Zeeman saturation. The same effects occur if the whole band is calculated.

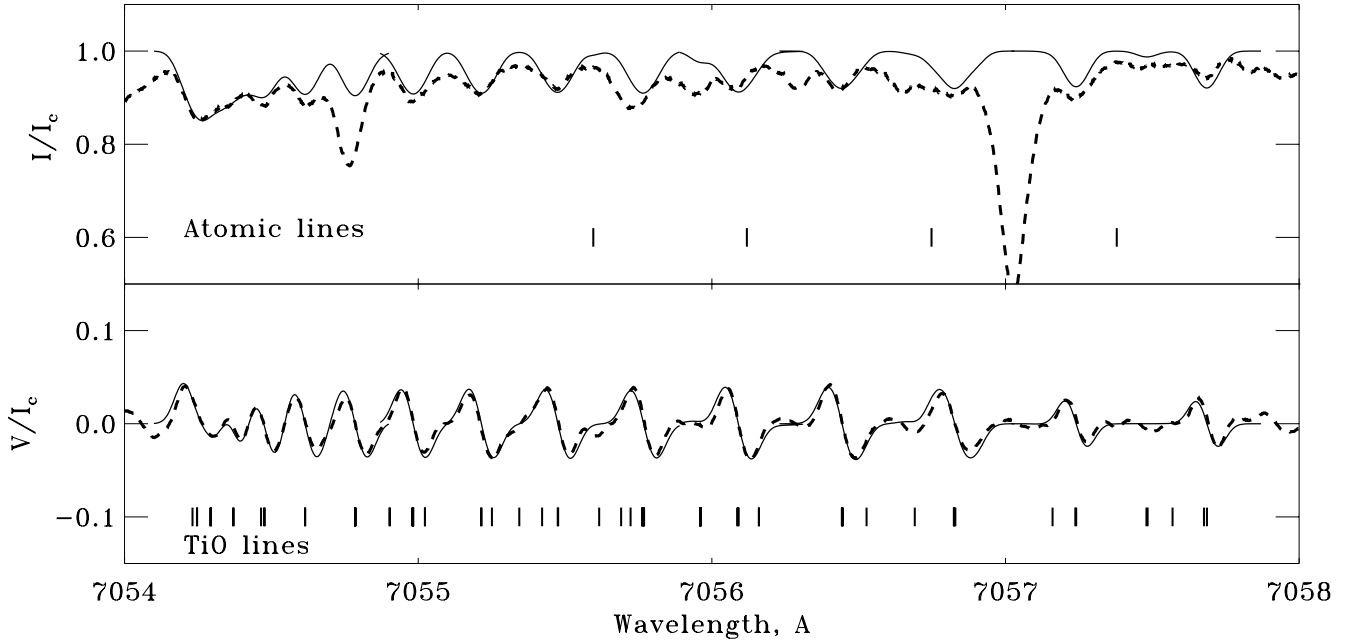


**Fig. 1.** The TiO  $\gamma(0,0)R_3$  band head in a sunspot. Calculated and observed Stokes  $I$  and  $V$  are represented by solid and dashed lines, respectively. The field strength underlying the spectral synthesis is 3 kG, the filling factor is 0.75, and the magnetic vector is directed along the line of sight. Vertical dashes indicate positions of lines included in the spectral synthesis. The two strongest absorption features seen in Stokes  $I$  are water lines produced in the Earth's atmosphere.

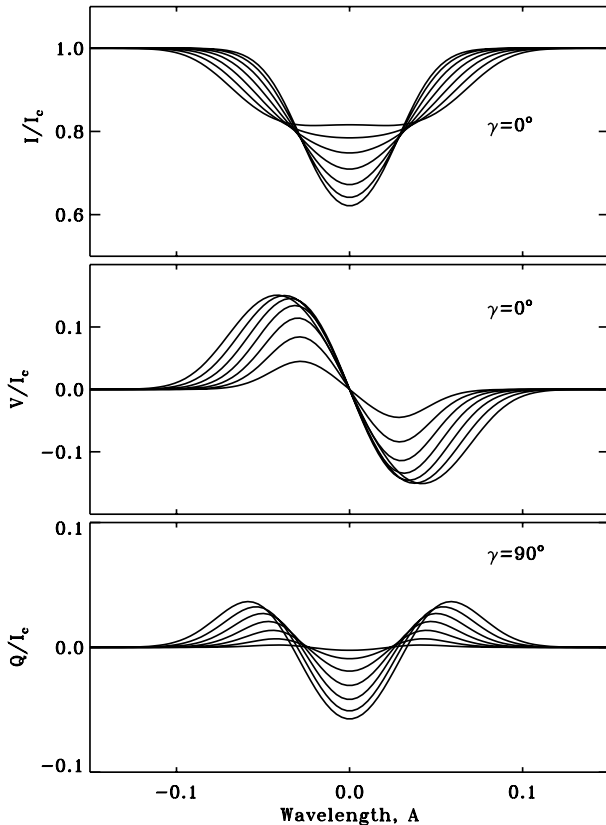


**Fig. 2.** Stokes  $I$ ,  $V$  and  $Q$  profiles of the TiO  $\gamma(0,0)R_3(10)$  line with an effective Landé factor of 0.4 at magnetic field strengths of 0.5–3.5 kG calculated with a step of 0.5 kG. An angle between the field vector and the line of sight of  $0^\circ$  and  $90^\circ$  has been chosen. Note that the Stokes  $Q$  signal is at least 3 times weaker than that of Stokes  $V$ .

### 3.1.2. The TiO $\gamma$ -system in starspots

The  $\gamma(0,0)R_3$  band head is, together with other band heads, observed in starspots (e.g., Ramsey & Nations 1980). It is interesting therefore to estimate the magnitude of the polarization signal from the band under stellar conditions. The most important factors determining the signal are the field strength, spectral resolution, stellar rotation rate, ratio of the continuum surface flux between the spot and the photosphere as well as the excess filling factor of spots of the dominant polarity on the visible stellar disk over the filling factor of spots with the opposite polarity. In Fig. 3 we present the synthesis of the band head at a resolution of  $0.07 \text{ \AA}$  (resolving power  $R = 100\,000$ ) broadened with two rates of stellar rotation:  $v \sin i$  of 2.5 and  $5 \text{ km s}^{-1}$ . The model underlying the computation has  $B = 3000 \text{ G}$ ,  $T_{\text{spot}} = 3750 \text{ K}$  and  $\log g = 4.5$ . Cooler spots will give stronger signal. The inclination  $\gamma$  and azimuthal  $\phi$  angles of the magnetic field employed are marked in each panel. To enhance visibility of Stokes  $V$  and  $Q$  different values of  $\gamma$  are used for the upper two frames ( $\gamma = 0^\circ$ ) than for the lower one ( $\gamma = 90^\circ$ ).

The resulting maximum line depth (Stokes  $I$ ) reached at the band head is 0.4–0.6. The maximum Stokes  $V$  amplitudes are 0.1 and 0.06 for  $v \sin i$  of 2.5 and  $5 \text{ km s}^{-1}$ , respectively, in units of the continuum intensity. Note that the Stokes  $V$  amplitude decreases more rapidly with spectral smearing than the Stokes  $I$  line depth (cf., Solanki & Stenflo 1986). Stokes  $V$  suffers particularly when the lines are closely spaced. Thus, shortward of  $7055 \text{ \AA}$  only a single Stokes  $V$  peak survives for a  $5 \text{ km s}^{-1} v \sin i$ .

If the magnetic field vector is perpendicular to the line of sight ( $\gamma = 90^\circ$ ), relatively strong Stokes  $Q$  and  $U$  can be

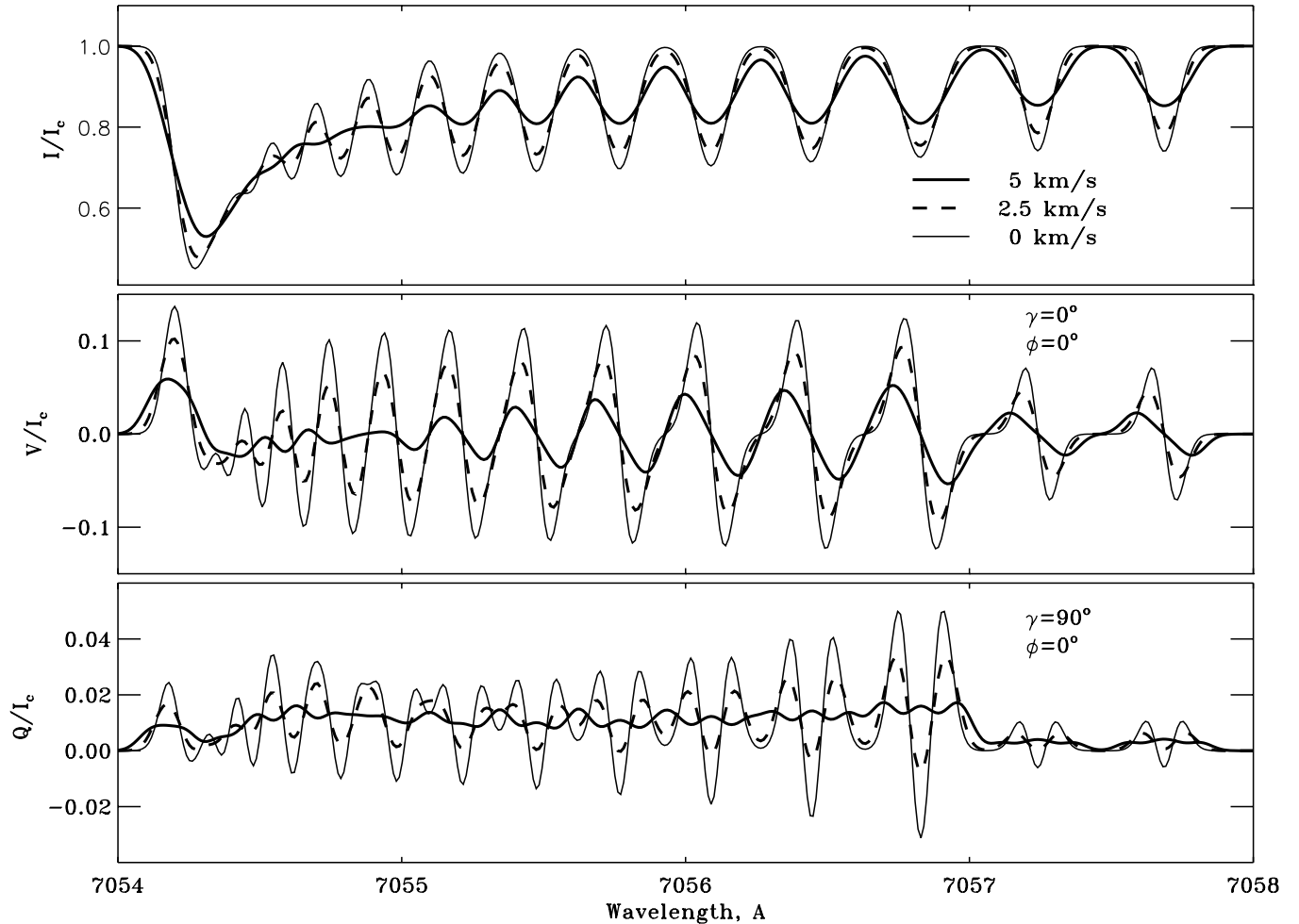


**Fig. 3.** The TiO  $\gamma(0,0) R_3$  band head in a starspot with a field strength of 3 kG. The thin solid line represents synthetic Stokes profiles convolved with only an instrumental profile of  $0.07 \text{ \AA}$  ( $R = 100\,000$ ), while thick dashed and solid lines show the spectra broadened in addition by stellar rotation with a  $v \sin i$  of 2.5 and  $5 \text{ km s}^{-1}$ , respectively. The spectra are calculated for different angles of the magnetic field vector: for an angle between the vector and the line of sight  $\gamma = 0^\circ, 90^\circ$  and for the azimuthal angle  $\phi = 0^\circ$ .

observed in the band (see two lower plots in Fig. 3). The maximum amplitudes in these Stokes parameters at  $v \sin i$  of 2.5 and  $5 \text{ km s}^{-1}$  are 0.03 and 0.02, respectively. Note that a clear signature of the broad-band linear polarization is noticeable at  $v \sin i = 5 \text{ km s}^{-1}$ . The net linear polarization signal integrated over a window 7054–7057  $\text{\AA}$  is 1.1%, almost independent of the  $v \sin i$  value.

For a real starspot the calculated amplitudes should be further reduced in accordance with the continuum flux ratio, which is 0.3 at 7054  $\text{\AA}$  for  $T_{\text{phot}} = 4750 \text{ K}$ , and the net filling factor of the dominant polarity starspots. While the total starspot filling factor can be as high as 50% (Neff et al. 1995), little is known about the polarity of starspots. An estimate of the influence of all these factors, except the polarity distribution, can be made from the fact that the observed central depth of the band can be as large as 0.1 measured relative to the total continuum level in some very active stars. For instance, an estimate for the observed Stokes  $V/I_c$  signal from starspots in the TiO band of 0.3% was obtained for the active RS CVn-type star IM Peg under the assumption that the dominant starspot on a Doppler image of the star is a

unipolar monolithic structure (Berdyugina 2002). The registration of such a signal is (marginally) achievable with current stellar spectropolarimetric facilities for a sample of active stars, if e.g., the starspots resolved by Doppler imaging are unipolar. By appropriately combining the Stokes  $V$  signatures from all the lines near the band head a reasonable S/N ratio should be achievable. The analysis of such observations can provide the first direct measurement of the magnetic field inside spatially unresolved starspots and, thus, provide the first probe of the internal structure of starspots.

### 3.1.3. Other TiO band systems

*$\gamma'$ -system.* Because of the perturbation due to spin uncoupling, lines of this system in the  $P_1, P_3$  and  $R_1, R_3$  branches display an unusual behaviour: their magnetic sensitivity increases with rotational number, while normally it should decrease (Paper I). This implies that all lines of the system observed between 6150  $\text{\AA}$  and 6400  $\text{\AA}$  are magnetically sensitive, with an average effective Landé factor  $g_{\text{eff}} = 0.5$ .

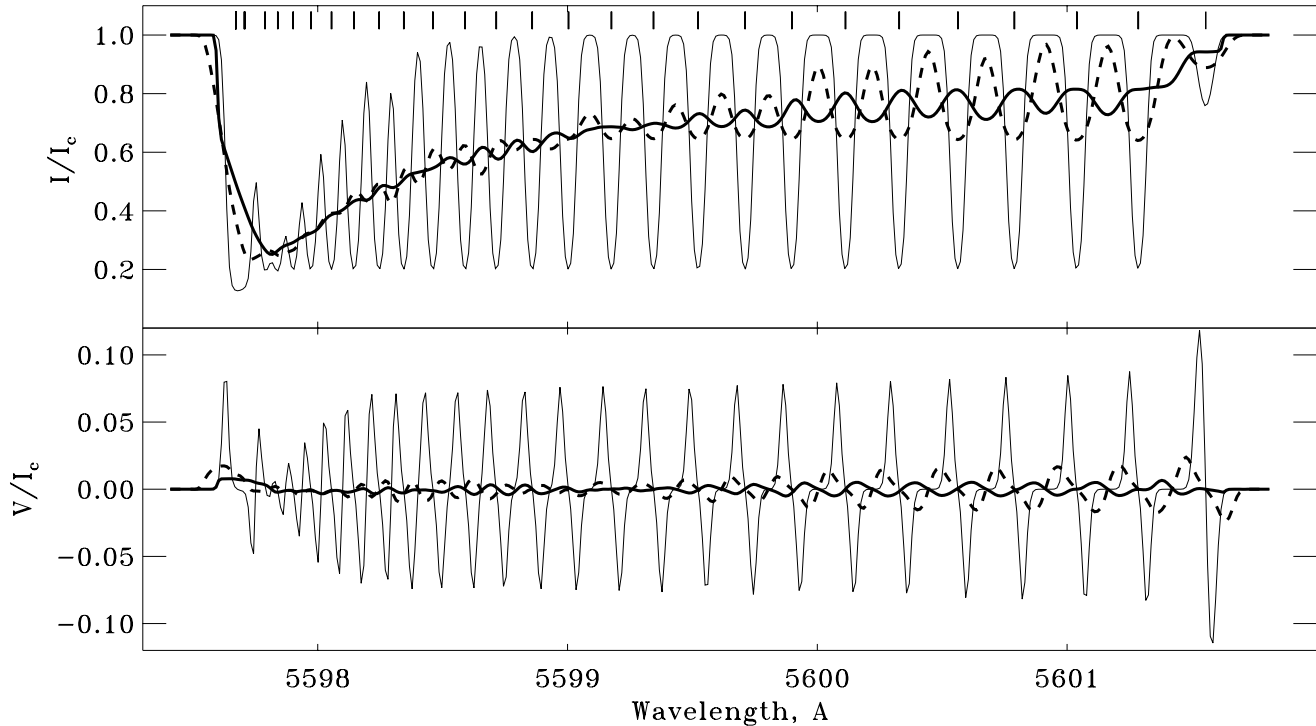


**Fig. 4.** Synthetic Stokes  $I$  and  $V$  of the TiO  $\beta(0,0)R$  band head. The thin solid line represents synthetic Stokes  $I$  and  $V$  that have undergone only an instrumental broadening of  $0.05 \text{ \AA}$  ( $R = 100\,000$ ), while thick dashed and solid lines show the spectra broadened in addition by the effect of stellar rotation with a  $v \sin i$  of  $2.5$  and  $5 \text{ km s}^{-1}$ , respectively.

*$\alpha$ -system.* In Paper I we showed that effective Landé factors of lines of allowed branches of this system are close to zero and the perturbation due to spin uncoupling is too small to increase them significantly. This is confirmed by observations of sunspot spectra, where lines of this system appear as very narrow features in Stokes  $I$  and give no Stokes  $V$  signal (Wallace et al. 2000; Berdyugina et al. 2000). They, however, heavily blend other lines at  $4000\text{--}7000 \text{ \AA}$  and, therefore, reduce and distort the polarization signals of those.

*$\beta$ -system.* Three branches of the system at  $5597\text{--}5740 \text{ \AA}$  are clearly observed in the sunspot spectrum (Wallace et al. 2000). These are  $R(0,0)$ ,  $Q(0,0)$  and  $R(1,1)$ . As was shown in Paper I,  $R$  branches show higher magnetic sensitivity than  $Q$  branches. Stokes  $I$  and  $V$  profiles for the  $R(0,0)$  branch are shown in Fig. 4, calculated for the same parameters as the  $\gamma(0,0)R_3$  branch plotted in the two upper frames of Fig. 3. In the band head lines are so closely spaced that the Stokes  $V$  signal is canceled out except for a single peak. It increases, however, further from the head, reaching values almost as large as the  $\gamma(0,0)R_3$  band. Broadening due to stellar rotation severely reduces the Stokes  $V$  signal of the  $R(0,0)$  branch of the  $\beta$ -system, however. The reason is basically the close spacing of the lines, which leads to severe blending and cancellation. The maximum values reached for  $v \sin i = 2.5$  and  $5 \text{ km s}^{-1}$  are  $4\%$  and  $2\%$ , respectively (both in units of continuum intensity).

*$\delta$ -system.* The relatively strong  $(0,0)$  band head in the  $R$  branch of the system is observed in sunspot spectra at  $8860 \text{ \AA}$ . It develops significantly in spectra of cool stars of

spectral types K4 to M6 (Ramsey 1981). Lines of the  $R$  branch possess high enough Zeeman sensitivity to produce significant Stokes  $V$  signals in sunspots and starspots (Paper I) and, therefore, could be useful for diagnosis of magnetic fields in cool stars.

### 3.2. OH

Lines of vibration-rotation bands of OH in the ground state  $X^2\Pi$  (Meinel system) cover a wide spectral region in the infrared: the first-overtone ( $\Delta v = 2$ ) sequence is found in the range  $1.5\text{--}1.8 \mu\text{m}$ , and the fundamental ( $\Delta v = 1$ ) sequence in the range  $3.1\text{--}4.2 \mu\text{m}$  (Wallace & Livingston 1993).

The reversal of the sign of the circular polarization produced by some molecular lines compared to atomic or other molecular lines was a puzzle for a long time (e.g. Nicholson 1938; Harvey 1973, 1985; Rüedi et al. 1995). In the spectrum of a sunspot umbra Harvey (1985) discovered that lines of the same OH band and of approximately the same strength exhibit opposite polarities. Portions of an FTS (Fourier Transform Spectrometer) spectrum of a sunspot umbra is plotted in Fig. 5, where 4 OH lines from the  $(2,0)$  band and 2 lines from the  $(3,1)$  band with opposite polarities are marked. The complete data set is described and discussed by Rüedi et al. (1995).

The opposite signs of the OH Stokes  $V$  profiles are explained by the fact that the lines have equal but opposite effective Landé factors (Paper I; Berdyugina & Solanki 2001): reversed polarity is exhibited by the lines belonging to the  $P_2$  sub-branch ( $g_{\text{eff}} < 0$ ), while the  $P_1$  transitions have the

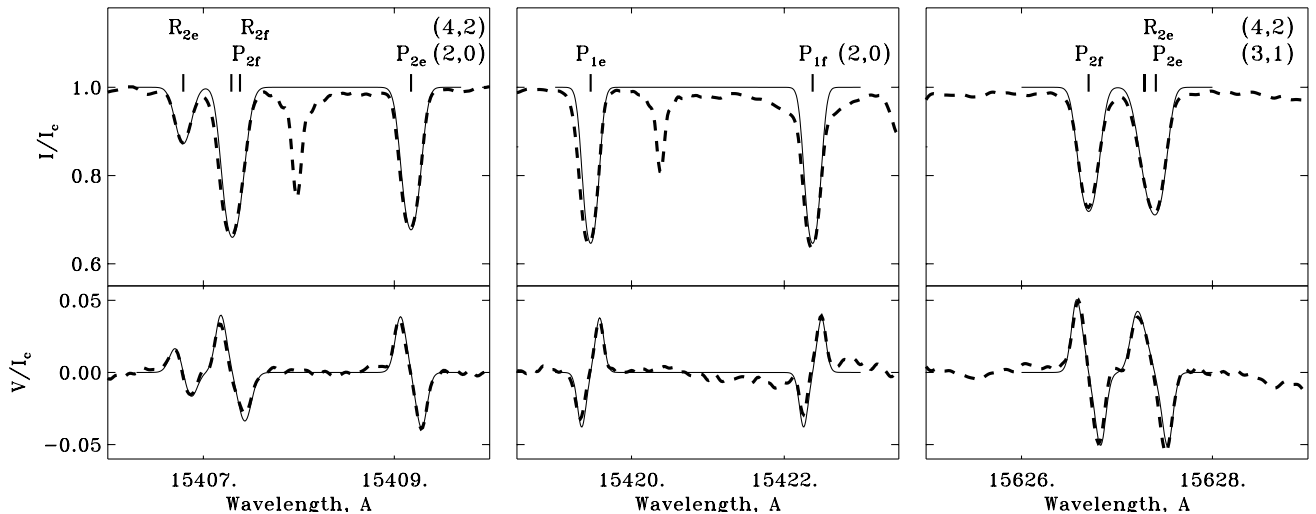


**Fig. 5.** Stokes  $I$  and  $V$  spectra of the OH lines with polarization patterns having opposite sign. Dashed lines: observed in a sunspot, solid lines: synthesized assuming a longitudinal field with a strength of 2.5 kG. Note that the magnetic field in the spot is directed away from the observer and, thus, it is the left and right pairs of lines that show reversed polarization.

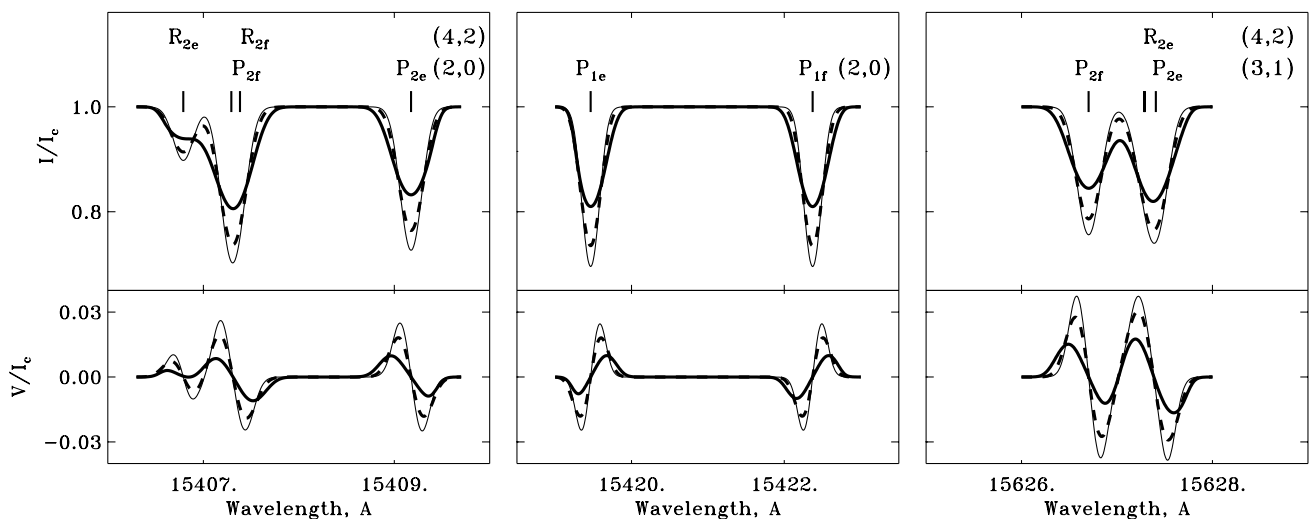


**Fig. 6.** The same as Fig. 3 for the OH lines at a spectral resolution of  $0.15 \text{ \AA}$  ( $R = 100\,000$ ) and  $v \sin i$  values of 2.5 and  $5 \text{ km s}^{-1}$ .

normal sign of the polarity ( $g_{\text{eff}} > 0$ ). The synthetic Stokes profiles of OH lines calculated with the theory of the intermediate Hund's case (a-b) presented in Paper I successfully fit observed profiles of these lines in the umbral spectrum (Fig. 5; Berdyugina & Solanki 2001). Our calculations show that the  $R_1$  and  $R_2$  transitions are also well reproduced; see the  $R_{2e}$  line from the (4,2) band in the left frame of Fig. 5 or the good fit to the asymmetric  $V$  profile at  $15\,627.5 \text{ \AA}$  formed by a blend of a  $R_{2e}$  and a  $P_{2e}$  transition. Such a behavior is typical for all OH lines from the Meinel system and also for pure rotational transitions in the ground state (Jennings, personal communication).

The synthesis of Zeeman-split OH lines also helps to improve the diagnostic capability of atomic lines. In sunspots, strong OH lines from the (3,1) band are observed in the vicinity of the Zeeman sensitive Fe I  $15\,648.5 \text{ \AA}$  line and are blended with Fe I  $15\,652.9 \text{ \AA}$ . Together, these two Fe I lines are the premier infrared diagnostics of the solar magnetic field (e.g.

Solanki et al. 1992) and are widely used. Inverting the Stokes parameters of the blending OH lines along with the Fe I lines greatly improves the reliability of magnetic, thermal and dynamic quantities deduced from these lines in sunspot umbrae (Berdyugina et al. 2003; Mathew et al. 2003).

The first detection of infrared OH lines from starspots was reported by O'Neal & Neff (1997). They observed an excess of OH absorption in the blend of the  $\Lambda$ -type doublet  $P_2(5.5)$  at  $15\,627 \text{ \AA}$  and interpreted it as a contribution from cool starspots. In order to see the effect of the starspot magnetic field in the OH lines, we synthesized the Stokes  $I$  and  $V$  profiles for a model with  $T_{\text{spot}} = 3750 \text{ K}$  and  $\log g = 4.5$  with a height-independent magnetic field strength of 2.5 kG. In Fig. 6 the profiles are plotted for a spectral resolution of  $0.15 \text{ \AA}$  (resolving power  $R = 100\,000$ ) and stellar rotation broadening of 0, 2.5 and  $5 \text{ km s}^{-1}$ . Again, the resulting Stokes profiles should be scaled by the continuum flux ratio (0.6 for  $T_{\text{phot}} = 4750 \text{ K}$  at  $15\,627 \text{ \AA}$ ) and the net spot filling factor. A measurable

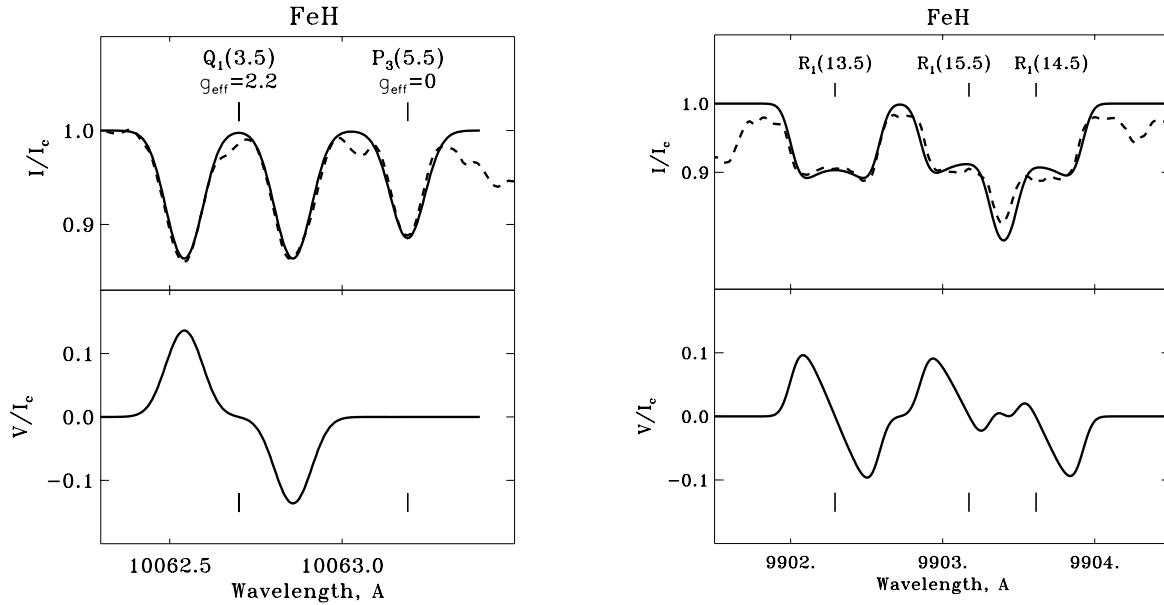


**Fig. 7.** Stokes  $I$  and  $V$  of sample FeH lines in a sunspot umbrae. Observations (dashed; only Stokes  $I$ ) are from Wallace et al. (1998). Synthetic Stokes profiles (solid) are calculated for a field strength of 3 kG. The zero-field positions of the lines are indicated by vertical dashes.

signal in Stokes  $V$  is only obtained if very low noise observations can be made. Hence, infrared OH lines can in principle also be a useful diagnostic of stellar magnetic fields, although in practice it may not be so easy to obtain data with the necessary high S/N ratio.

### 3.3. FeH

The calculation of the Zeeman effect in FeH lines of the infrared  $F^4\Delta - X^4\Delta$  system is made difficult by the fact that the required spin-orbit coupling constants of the two electronic states are not known. The magnetic sensitivity of many lines of this system is, however, remarkable, as can be seen from the sunspot observations made by Wallace et al. (1998). The same observations show also that the perturbation due to spin uncoupling is big, so that the behaviour of the Landé factors is similar to that of the TiO  $\gamma$ -system. With appropriate (empirically determined) spin-orbit coupling constants we can reproduce purely Stokes  $I$  observations, as shown in Fig. 7. We can predict the Stokes  $V$  signal as well. The fully split  $Q_1(3.5)$  line at 10062.7 Å, for instance, is potentially an excellent diagnostic of the umbral upper photosphere.

The power of the FeH lines as stellar magnetic field diagnostics was clearly demonstrated by Valenti et al. (2001). They detected the Zeeman broadening of FeH lines in an active M dwarf and, using the sunspot spectrum by Wallace et al. (1998), performed simple modeling of the stellar spectrum. Nevertheless, an accurate laboratory analysis of FeH is urgently needed.

### 3.4. CH

CH lines contributing to the so-called  $G$ -band spectral feature at about 4300 Å are found to be magnetically sensitive, especially those arising from the  $R_1$ ,  $P_2$  and  $Q_1$  branches

(Paper I). Lines of these branches are observed in the wavelength intervals 4133–4304 Å, 4328–4413 Å, 4270–4315 Å, respectively. The lines in these wavelength regions are however blended with atomic and other, less magnetically sensitive CH lines. The CH lines are very strong in both the solar photosphere and sunspot umbra (Wallace et al. 2000), although they become weaker at both higher and lower temperature. In Fig. 8 (upper panel) a spectral region with  $Q_1$  branch lines observed in a sunspot (Stokes  $I$  only, Wallace et al. 2000) is compared with spectra calculated for two atmosphere models with  $T_{\text{eff}} = 4000$  K and 4250 K. Note that the lines are stronger for  $T_{\text{eff}} = 4250$  K. Also, the Stokes  $V$  signal expected for a longitudinal magnetic field of 3 kG is shown in the lower panel. The strongest Stokes  $V/I_c$  signal from the CH lines is expected at 4311.2 Å, where signals from the lines (0,0)  $Q_1(6.5)$ , (1,1)  $Q_1(6.5)$  and (2,2)  $R_2(0.5)$  are constructively combined to produce a peak Stokes  $V/I_c$  value approaching 0.2 for  $T_{\text{eff}} = 4250$  K. In other blends the Stokes  $V/I_c$  signal is of the order of 0.1. The blending gives rise to very asymmetric  $V$  profiles in many cases.

## 4. Thermal molecular diagnostics

### 4.1. Number densities

The high temperature sensitivity of molecular number densities is seen from Eq. (7), where  $N_{AB} \propto \exp(\frac{D_0}{kT})$ . If we express  $D_0$  in eV, replace the exponent by  $10^{D_0/\theta}$ , where  $\theta = 5040/T$ , and neglect the temperature dependence of the partition functions, then we obtain a useful relation:

$$\frac{\Delta N_{AB}}{N_{AB}} \approx -\frac{\Delta T}{T}(1.5 + 2.3 \theta D_0). \quad (11)$$

From this relation we can estimate that an increase of the temperature by only 1%, i.e. 50 K, around 5000 K, results in a decrease of the number density of a molecule with  $D_0 = 10$  eV

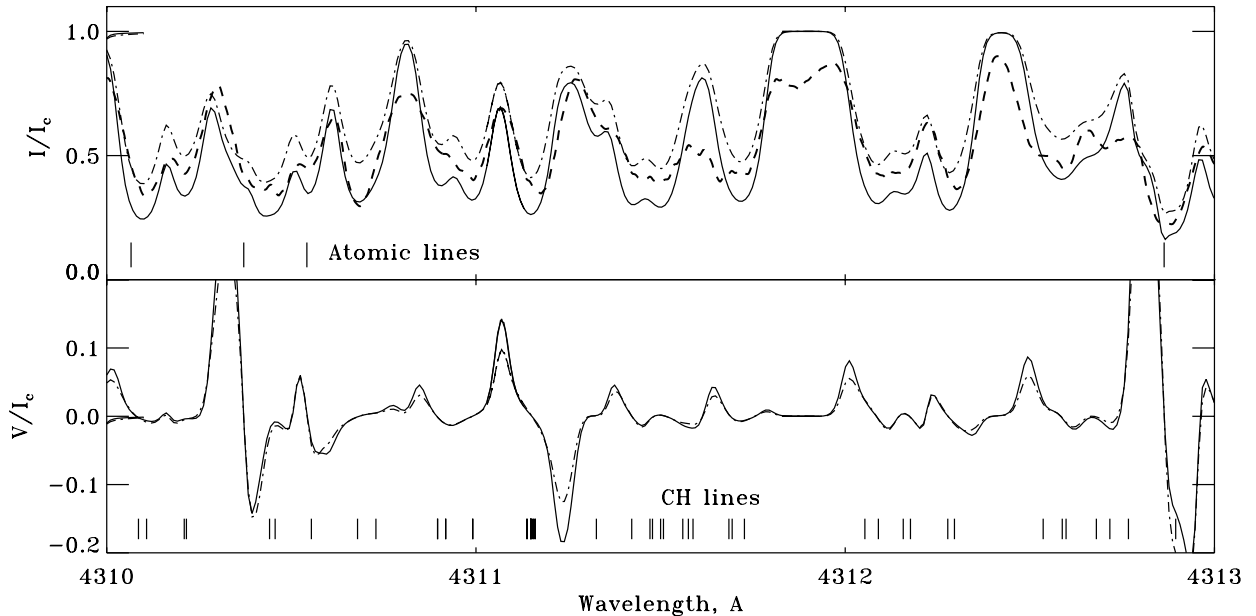


**Fig. 8.** CH lines from the A-X system in a sunspot. Calculated Stokes  $I$  and  $V$  for atmosphere models by Kurucz (1993) with  $T_{\text{eff}} = 4250$  K and  $4000$  K are represented by solid and dashed-dotted lines, respectively. Stokes  $I$  is compared with observations by Wallace et al. (1998), plotted dashed. The field strength underlying the spectral synthesis is  $3$  kG and the magnetic vector is directed along the line of sight. Vertical dashes indicate positions of lines included in the spectral synthesis.

by 25%! In this respect, CO ( $D_0 = 11$  eV) would be the most temperature sensitive molecule. Unfortunately its lines in the infrared are not magnetically sensitive. TiO (6.9 eV), CN (7.7 eV), OH (4.4 eV) and CH (3.5 eV) are also rather temperature sensitive and, as shown earlier, their optical transitions are good indicators of magnetic fields. MgH (1.3 eV) and FeH (1.6 eV) are not extremely sensitive to small temperature variations according to Eq. (11) under the simplifying approximations underlying it.

The temperature sensitivity of the molecules can be further judged from Figs. 9 and 10, which present molecular number densities for the models by Kurucz (1993) with  $T_{\text{eff}} = 5750 \pm 250$  K and  $4000 \pm 250$  K corresponding to the solar photosphere and a sunspot or a cool star, respectively.

In addition to high temperature sensitivity, molecules are also sensitive to pressure variations. As seen from Eq. (7):

$$N_{AB} \propto N_A N_B, \quad (12)$$

which turns to be further proportional to the square of the hydrogen density. For instance, metal hydrides such as MgH, FeH, CaH, etc. are found to be highly pressure sensitive (cf. Bell et al. 1985; Berdyugina & Savanov 1992; Schiavon et al. 1997).

Note that the number densities provide only a part of the information needed to judge the usefulness of a particular molecular spectrum as a temperature diagnostic. Individual lines need to be considered, since their strength is an additional important parameter.

#### 4.2. Contribution and response functions

The depth in the atmosphere at which a spectral line is formed, or rather the range of depths over which it is sensitive to some

physical parameter is an important quantity when using spectral lines for probing solar and stellar atmospheres. To quantify the formation depth range, we use two complementary concepts, contribution functions (CF) and response functions (RF). The former, calculated for the relative line depression, represents a depth-dependent function illustrating the relative contribution of different layers to the formation of the line. It can be calculated for all Stokes parameters. A detailed description of the calculated functions is given by Grossmann-Doerth et al. (1988) and Solanki & Bruls (1994). The response function is useful for empirical diagnostics of atmospheric parameters. It illustrates the effect on the line profile of perturbations in a given atmospheric parameter at different depths. For every parameter, e.g. velocity, temperature, magnetic field strength, a different response function is needed. Response functions for Stokes profiles have been given by Landi Degl'Innocenti & Landolfi (1982, 1983), cf. Grossmann-Doerth et al. (1988), Ruiz Cobo & del Toro Iniesta (1994).

In Figs. 11 and 12 we present Stokes  $I$  line depression contribution functions at the cores of a sample of molecular lines for the radiative equilibrium model atmospheres by Kurucz (1993) with  $T_{\text{eff}} = 5750$  K and  $3750$  K, which represent the solar photosphere and a sunspot or a cool star (M dwarf). The line sample included CH A-X(0,0)  $Q_2$ (12.5), MgH A-X(0,0)  $Q_1$ (23.5), CN red system (0,0)  $R_1$ (19.5), CN violet system (0,0)  $P_2$ (28.5), OH (2,0)  $P_2$ (9.5), and TiO  $\gamma$ (0,0)  $R_3$ (21). From the shapes and relative amplitudes of the functions we conclude that in the solar atmosphere CH and CN violet system lines are relatively strong and effectively formed at optical depths  $\log \tau_{5000} = -1.5$ . The cores of the calculated lines are formed over roughly the same range of depths, differences being attributable to differences in line strength (Fig. 11). Not plotted is the

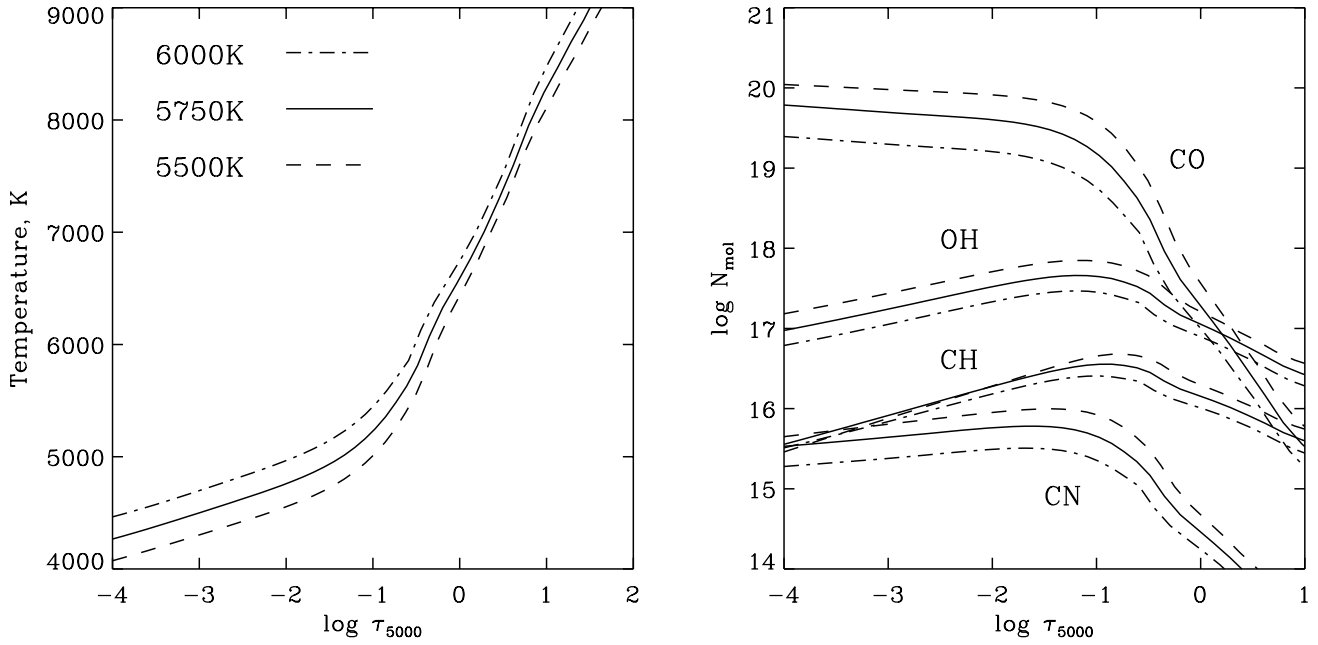


**Fig. 9.** On the left, temperature stratification of three atmospheric models by Kurucz (1993) with  $T_{\text{eff}} = 5750 \pm 250$  K representing the solar photosphere with temperature fluctuations. On the right, the corresponding number densities of 4 molecules relevant for these temperatures.

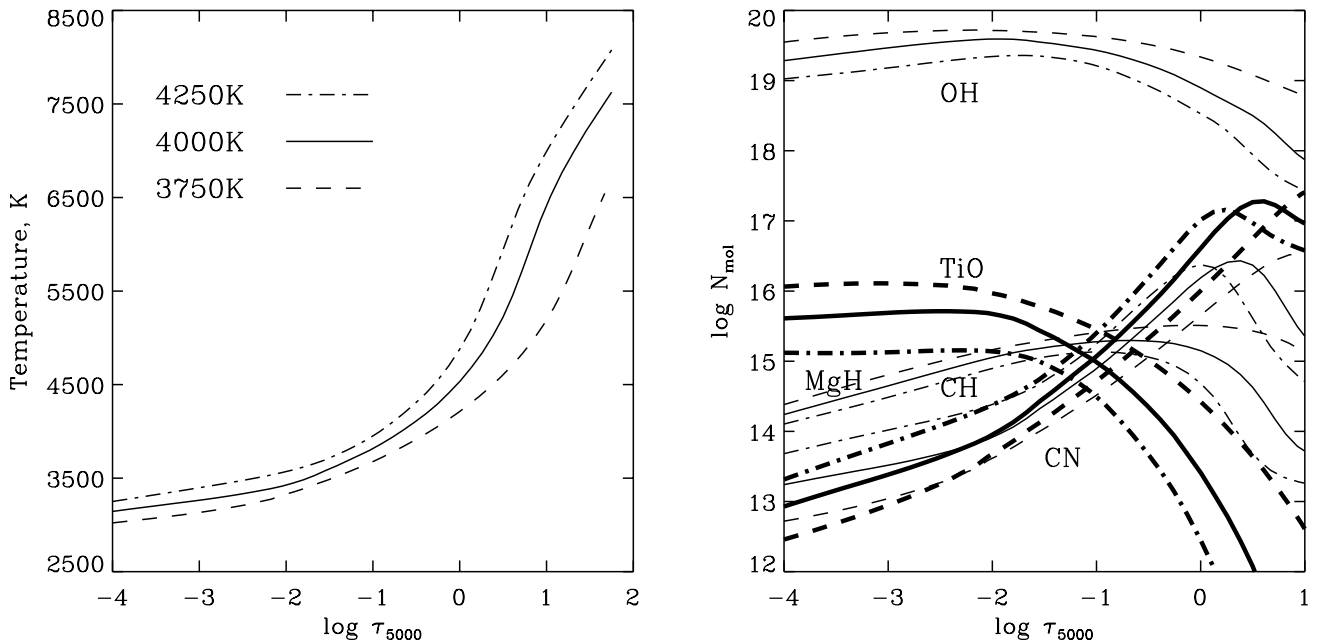


**Fig. 10.** On the left, temperature stratification of three models with  $T_{\text{eff}} = 4000 \pm 250$  K representing a sunspot or a cool stellar photosphere with temperature fluctuations. On the right, the corresponding molecular number densities. The curves representing TiO and CH are plotted thick in order to distinguish them from the curves representing MgH and CN.

contribution function of a strong CO ro-vibrational line which is formed higher in the atmosphere (Ayres et al. 1986; Solanki et al. 1994). In sunspots, or cool stars, TiO, MgH and OH become more important and are formed higher up, at  $\log \tau_{5000} = -2$ , while CH and CN lines are formed very deep in the atmosphere, at  $\log \tau_{5000} = -0.5$  or deeper. This difference in formation depth can already be sensed in Fig. 10, where the rapid increase of CN and CH number densities with depth down to the continuum forming layers is seen. This suggests that at least in cool atmospheres using lines of different molecules, having

very different formation depths, can provide strong constraints on the temperature stratification of the atmosphere.

If many lines from the same molecular band are used, the atmosphere can be sampled on a fine depth grid, since relative line strengths in the band are usually known accurately. The lines in a band are formed at depths lying close to each other and therefore cover a range of depths in very fine steps. In Fig. 13 we present contribution functions calculated for 30 lines in the TiO  $\gamma(0,0)R_3$  band head (solid curves). They effectively cover the depth range  $\log \tau_{5000} = -3$  to  $-1$ . A wider

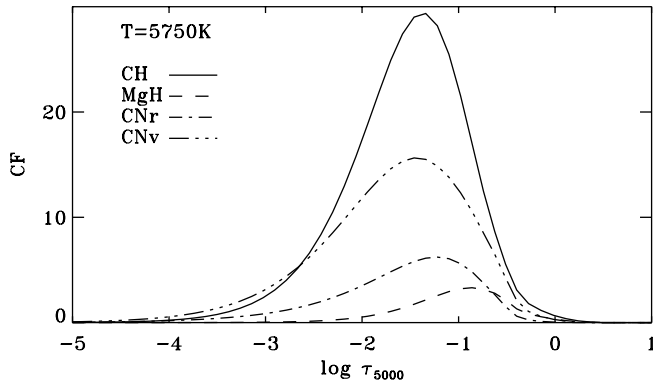


**Fig. 11.** Normalized Stokes  $I$  line depression contribution functions of a sample of molecular lines for the model atmosphere with  $T_{\text{eff}} = 5750$  K.

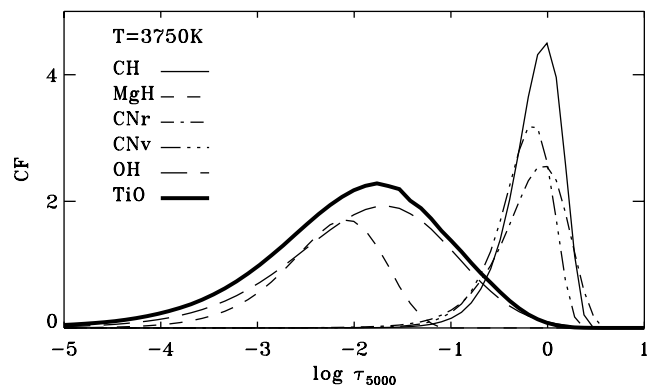


**Fig. 12.** The same as Fig. 11 for the model atmosphere with  $T_{\text{eff}} = 3750$  K.

depth range is covered by 30 MgH lines from the (0,0)  $Q_1$  band,  $\log \tau_{5000} = -3$  to 0 (dashed curves). Using such a sample of lines may provide an interesting diagnostic for atmospheric stratification. The different lines in a band sample the atmosphere at regular and finely spaced intervals as they are formed in slightly different depth ranges, so that, e.g., an inversion involving a selection of lines in a band should be able to return the atmospheric stratification over the range of formation depth of the band with considerable accuracy. Also, in the case of TiO, the fact that a large number of lines sample almost the same layers of the atmosphere means that they can be combined to increase the robustness of the diagnostic by increasing the S/N ratio.

The constraints provided by molecular lines for the temperature and magnetic field stratification can be further investigated with the help of response functions. In Fig. 14 the RF for temperature and magnetic field strength are shown for Stokes  $I$  (at the line core) and Stokes  $V$  (at the peak of the blue lobe), respectively, of the TiO  $\gamma(0,0)R_3(16)$  line. The shapes of the functions are similar to each other, as well as to the CF shown in Fig. 13. This means that it is at the effective line formation depth that the line core (and the peak in Stokes  $V$ ) provide the strongest constraint on the temperature and magnetic field. Thus, the contribution functions in Figs. 11 and 12 also provide a good indication of the temperature and magnetic field strength response functions of the computed lines. This

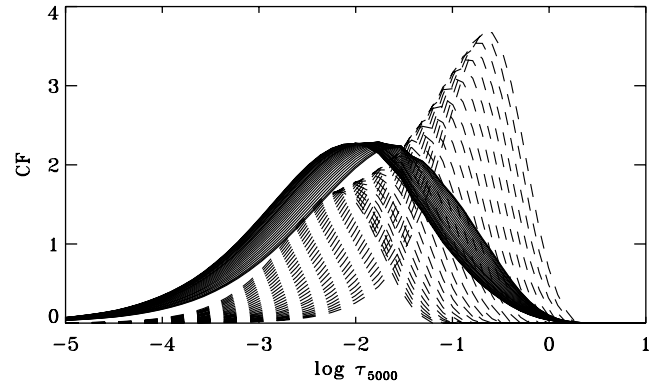


**Fig. 13.** The same as Fig. 11 for the TiO  $\gamma(0,0)R_3$  band head (solid lines) and MgH A–X (0,0)  $Q_1$  band (dashed lines). The model atmosphere with  $T_{\text{eff}} = 3750$  K has been employed.

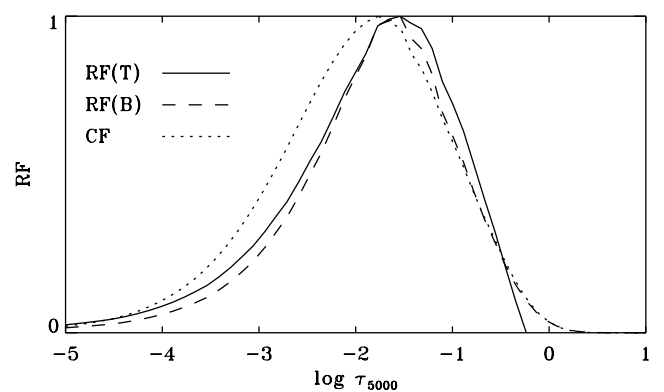


**Fig. 14.** Normalized temperature response function for Stokes  $I$  and magnetic field response function for Stokes  $V$  of the TiO  $\gamma(0,0)R_3(16)$  line. The model atmosphere with  $T_{\text{eff}} = 3750$  K has been employed. The contribution function for the line centre from Fig. 12 is shown for comparison.

behaviour is found to be common among the sample of calculated molecular lines.

#### 4.3. Imaging in molecular bands

Images of the solar photosphere made in  $G$ -band radiation strikingly reveal the so-called  $G$ -band bright points, which correspond to small-scale magnetic structures within intergranular lanes (cf. Berger & Title 2001 and references therein). As was shown recently, the observed high contrast of the  $G$ -band bright points can be explained by the high temperature sensitivity of CH lines, caused by the increased dissociation of CH molecules at temperatures above photospheric (Steiner et al. 2001; Sánchez Almeida et al. 2001; Schüssler et al. 2003). The density of CH lines is very high in the  $G$ -band. The high temperature of the small-scale magnetic structures reduces the number of CH molecules via dissociation, and the features look brighter.

Similar effects can be observed in other molecular bands. For instance, the earlier, lower resolution images made using filters centred on the CN violet band head at 3883 Å by Chapman (1970) and Sheeley (1971) also show a high contrast between small-scale magnetic features and their surroundings.

In Fig. 15 we present calculations of the equivalent widths of a sample of molecular lines observed in quiet Sun and sunspot spectra for different atmosphere models (Kurucz 1993). The sample of lines used is the same as in Sect. 4.2 except the OH line. Here we present the (0,0)  $Q_1$  (20.5) line from the ultraviolet A–X system at 3150 Å. The latter is chosen because UV OH lines are very strong in both the solar photosphere and umbrae and may be of considerable interest for high-contrast imaging.

Molecular lines which are strongest at about 5000 K (Fig. 15) are useful for studying inhomogeneities in the temperature range 5000 K to 7000 K and for imaging of small-scale magnetic fields in the solar photosphere (plage and network regions). In addition to CH lines from the A–X system, these are violet CN and ultraviolet OH lines at 3883 Å and 3150 Å, respectively. The dissociation equilibria of CN and OH are similar to that of CH and one expects a similar brightening in their bands.

Molecular lines which are strongest at about 3500 K (Fig. 15) are useful for studying temperature inhomogeneities in sunspots. For instance, umbral dots would be seen at higher contrast if observed in the TiO or OH band heads. An experiment recently made with a filter centred at the TiO 7054 Å band head has confirmed this expectation (Berger & Berdyugina 2003).

In order to estimate the expected contrast of possible temperature inhomogeneities in sunspots and the photosphere, we calculate synthetic spectra for 4 spectral regions dominated by lines of CH, CN, OH and TiO: 4295–4315 Å, 3870–3885 Å, 3120–3130 Å, and 7051–7063 Å, respectively. The synthesis accounts also for atomic and other molecular lines which are stronger than 0.01 in Stokes  $I/I_c$ . With spectra calculated for a set of atmosphere models by Kurucz (1993) we define the contrast in the local continuum,  $C_c$ , and in the band,  $C_b$ , as follows:

$$C_c = \frac{I_c - I_{0,c}}{I_{0,c}}, \quad (13)$$

$$C_b = \frac{I_b - I_{0,b}}{I_{0,b}}, \quad (14)$$

where  $I$  denotes the intensity integrated over a given wavelength interval. The intensity  $I_0$  is calculated for a model chosen for normalization. For the photosphere, it is the model with  $T_{\text{eff}} = 5750$  K. For a sunspot, the models with  $T_{\text{eff}} = 5000$  K and  $T_{\text{eff}} = 3750$  K are chosen, to represent the average temperature of penumbrae and the coolest parts of umbrae, respectively. The resulting contrast in the 4 molecular bands is shown in Fig. 16 as a function of temperature.

In the photosphere, the contrast in molecular bands is significantly higher than that in the local continuum, except the TiO band region where the contrast is the same since no TiO lines are formed in the photosphere. The best contrast of temperature inhomogeneities with respect to the average brightness of the photosphere is expected to be observed in the CN band, while the CH and OH bands produce similar results. The superior contrast achieved around the CN band-head is probably due to high dissociation energy of CN and high density of lines in the band.

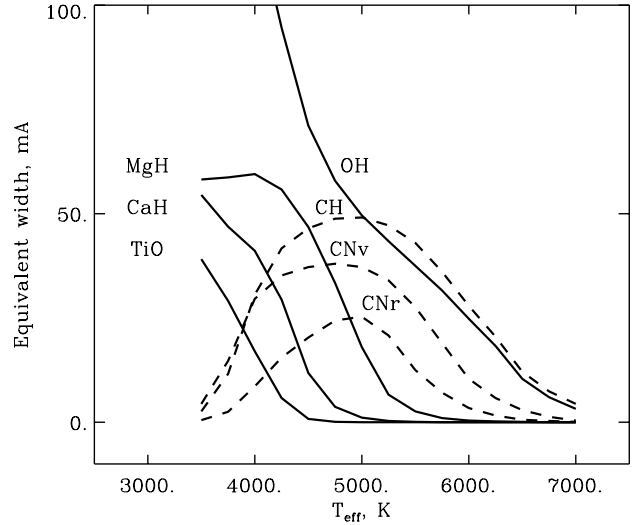


**Fig. 15.** Equivalent widths of a sample of molecular lines observed in quiet Sun and sunspot spectra for radiative equilibrium atmosphere models.

In a penumbra, as in the photosphere, the molecular bands show higher contrast than the continuum. Here, however, the best contrast is achieved in the CN and OH bands, while the CH band shows somewhat lower contrast.

In an umbra, the contrast in the TiO band is significantly higher than that in the local continuum, that was confirmed by recent observations (Berger & Berdyugina 2003). The CN, CH and OH bands show even higher contrast, mainly because they are observed at shorter wavelengths. In practice, due to the rapid increase of straylight from penumbra and quiet Sun with decreasing wavelength, we expect images made in the TiO band to have a similar or even better effective contrast. Note that the continuum, which apparently gives the highest contrast, is not observable in umbrae at shorter wavelengths because of heavy line absorption.

## 5. Conclusions

Molecular spectral lines provide an approach to studying sunspot umbrae, starspots and cool stars that in many ways complements the traditionally employed atomic lines. Molecular lines have been or can profitably be used to probe cool gas, e.g., in the chromosphere (e.g., Ayres & Testerman 1981; Ayres et al. 1986; Solanki et al. 1994; Uitenbroek et al. 1994), in the umbrae of sunspots (e.g., Sotirovski 1972; Boyer 1978; Wöhl 1971) or on stars and in starspots (e.g., Ramsey & Nations 1980; Neff et al. 1995; O’Neal et al. 1996). Due to their high temperature sensitivity molecular lines provide enhanced contrast in images. So far, with only a few exceptions (e.g., Valenti et al. 2001) molecular diagnostics have been restricted to the thermodynamic properties of solar and stellar atmospheres.

Here we have studied the diagnostic capabilities of lines of various molecules including also their sensitivity to the magnetic field via the Zeeman effect. We have described the synthesis of molecular Stokes parameters, including their radiative transfer under the assumptions of local thermodynamic

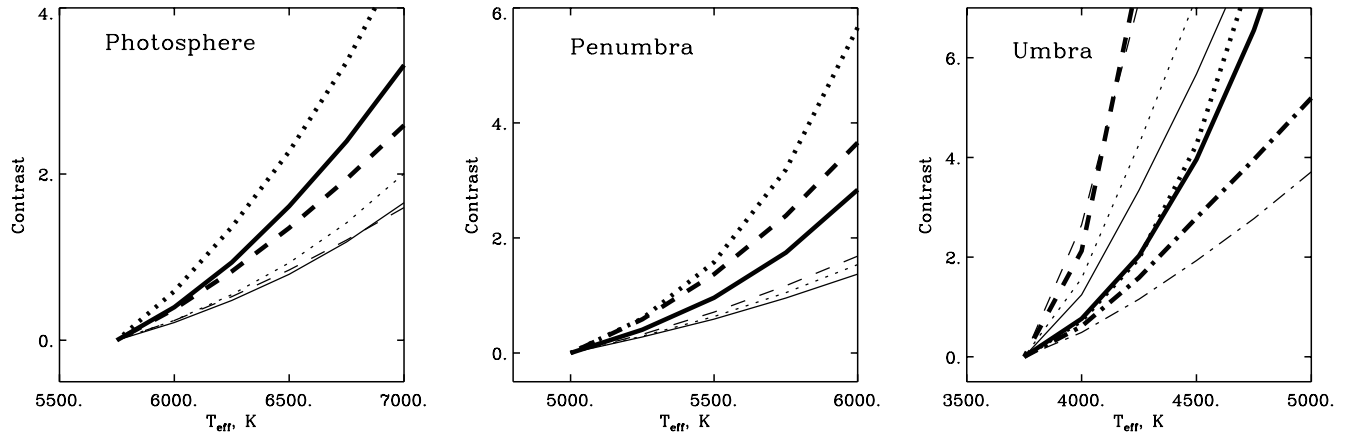


**Fig. 16.** Contrast of bright structures in the photosphere and in a sunspot penumbra and umbra, assuming radiative equilibrium models. Thick and thin curves denote the contrast in molecular bands and the local continuum, respectively. Solid, dotted, dashed and dashed-dotted lines represent calculations for CH at 4300 Å, CN at 3880 Å, OH at 3120 Å, and TiO at 7060 Å, respectively. TiO has not been plotted for the photosphere and penumbra, since the TiO lines are extremely weak there.

equilibrium and chemical equilibrium. We have discussed the validity of the equilibrium assumptions and concluded that in most cases they are adequate. We have studied the magnetic diagnostic capabilities of TiO, OH, FeH and CH lines observed in solar and cool star spectra and obtained the following results:

- The TiO  $\gamma$ -system (0,0) $R_3$  band head at 7054 Å is one of the best molecular diagnostics of the magnetic field in sunspot umbrae and starspots. The Stokes  $V$  signal in the band can be as high as 15% for a longitudinal magnetic field of 2.5 kG. We demonstrated that using the perturbation theory of the molecular Zeeman effect described in Paper I significantly improves the fit to Stokes  $V$  observed in a sunspot as compared to unperturbed calculations. In starspots, the expected Stokes  $V$  signal is of the order of 0.3%. We also found that at stronger transverse magnetic fields the band shows considerable net linear polarization (1.1% at 3 kG). This can be used for diagnostics of strong magnetic fields on the surfaces of cool stars observed with low spectral resolution.
- The puzzling opposite sign circular polarization observed in infrared OH doublet lines is explained by the fact that the lines have equal but opposite effective Landé factors. The synthetic Stokes profiles successfully reproduced observed profiles of these lines in the umbral spectrum. In a sunspot umbra, the peak circular polarization in OH lines is of the order of 5%. In starspots, it may be reduced to 0.1% and, thus, will require very high S/N data to be reliably used.
- Infrared FeH lines are excellent diagnostics of the umbral magnetic field. With appropriate (empirically determined) spin-orbit coupling constants we were able to reproduce remarkably strongly split Stokes  $I$  profiles observed in a sunspot spectrum. In order to make the power of the FeH diagnostics accessible, however, an accurate laboratory analysis of FeH is urgently needed.

We have also investigated the thermal diagnostic capabilities of molecular lines, by considering molecular number densities, contribution and response functions and the contrasts expected

from imaging in molecular bands. Based on our study, we conclude the following:

- Molecular number densities are very sensitive to small fluctuations of the temperature and gas pressure. Molecules with higher dissociation potentials demonstrate higher sensitivity to temperature variations.
- Analysis of contribution and response functions reveals that the lines in a particular band are formed at different depths and can provide strong constraints on the temperature stratification of the atmosphere. If many lines from the same molecular band are used, the atmosphere can be sampled on a fine depth grid.
- Imaging in molecular bands can help in studying the spatial fine structure of the photosphere and sunspots. In the photosphere, the best contrast of temperature inhomogeneities with respect to the average brightness of the photosphere is expected to be observed in the CN violet band head at 3883 Å. The CH and OH bands at 4300 Å and 3130 Å, respectively, produce similar results. In a penumbra, the best contrast is achieved in the CN and OH bands. For imaging umbral inhomogeneities, the TiO band head at 7055 Å is found to be very promising.

*Acknowledgements.* The NSO/Kitt Peak FTS data used here were produced by NSF/NOAO.

## References

- Anderson, L. S. 1989, *ApJ*, 339, 558  
 Ayres, T. R., & Testerman, L. 1981, *ApJ*, 245, 1124  
 Ayres, T. R., Testerman, L., & Brault, J. W. 1986, *ApJ*, 304, 542  
 Ayres, T. R., & Wiedemann, G. R. 1989, *ApJ*, 338, 1033  
 Bell, R. A., Edvardsson, B., & Gustafsson, B. 1985, *MNRAS*, 212, 497  
 Berdyugina, S. V. 2002, *AN*, 323, 192  
 Berdyugina, S. V., & Savanov, I. S. 1992, *Sov. Astr.*, 36, 425  
 Berdyugina, S. V., & Solanki, S. K. 2001, *A&A*, 380, L5  
 Berdyugina, S. V., & Solanki, S. K. 2002, *A&A*, 385, 701, Paper I  
 Berdyugina, S. V., Berdyugin, A. V., Ilyin, I., & Tuominen, I. 1999, *A&A*, 350, 626

- Berdyugina, S. V., Berdyugin, A. V., Ilyin, I., & Tuominen, I. 1999, *A&A*, 360, 272
- Berdyugina, S. V., Frutiger, C., Solanki, S. K., & Livingston, W. 2000, *A&A*, 364, L101
- Berdyugina, S. V., Solanki, S. K., & Lagg, A. 2003, in *The 12th Cambridge Workshop on Cool Stars, Stellar Systems, and the Sun*, ed. T. Ayres, & A. Brown, ASP Conf. Ser., in press
- Berger, T. E., & Title, A. M. 2001, *ApJ*, 553, 449
- Berger, T. E., & Berdyugina, S. V. 2003, *ApJ*, 589, L117
- Boyer, R. 1978, *A&A*, 69, 213
- Chapman, G. A. 1970, *Sol. Phys.*, 13, 78
- Donati, J.-F., Semel, M., Carter, B. D., Rees, D. E., & Collier Cameron, A. 1997, *MNRAS*, 291, 658
- Donati, J.-F., Collier Cameron, A., Hussain, G. A. J., & Semel, M. 1999, *MNRAS*, 302, 437
- Fowler, A. 1904, *Proc. R. Soc. London A*, 73, 219
- Frutiger, C., Solanki, S. K., Fligge, M., & Bruls, J. H. M. J. 2000, *A&A*, 358, 1109
- Grossmann-Doerth, U., Larsson, B., & Solanki, S. K. 1988, *A&A*, 204, 266
- Hale, G. E., & Adams, W. S. 1907, *ApJ*, 25, 45
- Hale, G. E., Adams, W. S., & Gale, H. G. 1906, *ApJ*, 24, 185
- Harvey, J. W. 1973, *Sol. Phys.*, 28, 43
- Harvey, J. W. 1985, in *Measurement of Solar Vector Magnetic Fields*, ed. M. J. Hagyard, NASA CP-2374, 109
- Johnson, H. R. 1994, in *IAU Coll. 146, Molecules in the Stellar Environment*, ed. U. G. Jørgensen (Springer Verlag), Lect. Not. Phys., 428, 234
- Kurucz, R. L. 1993, CD 13
- Lambert, D. L., & Mallia, E. A. 1972, *MNRAS*, 156, 337
- Landi Degl'Innocenti, E., & Landolfi, M. 1982, *Sol. Phys.*, 77, 13
- Landi Degl'Innocenti, E., & Landolfi, M. 1983, *Sol. Phys.*, 87, 221
- Mathew, S. K., Solanki, S. K., Lagg, A., et al. 2003, in *The Third International Workshop on "Solar Polarization"*, ed. J. Trujillo Bueno, & J. Sanchez Almeida, ASP Conf. Ser., 307, in press
- Neff, J. E., O'Neal, D., & Saar, S. H. 1995, *ApJ*, 452, 879
- O'Neal, D., Saar, S. H., & Neff, J. E. 1996, *ApJ*, 463, 766
- Nicholson, S. B. 1938, *PASP*, 50, 224
- Ram, R. S., Bernath, P. F., Dulick, M., & Wallace, L. 1999, *ApJS*, 122, 331
- Ram, R. S., Bernath, P. F., & Wallace, L. 1996, *ApJS*, 107, 443
- Ramsey, L. W. 1981, *AJ*, 86, 557
- Ramsey, L. W., & Nations, H. L. 1980, *ApJ*, L121
- Rees, D. E., Durrant, D. J., & Murphy, G. A. 1989, *ApJ*, 339, 1093
- Rüedi, I., Solanki, S. K., Livingston, W., & Harvey, J. 1995, *A&AS*, 113, 91
- Ruiz Cobo, B., & del Toro Iniesta, J. C. 1994, *A&A*, 283, 129
- Rutten, R. J. 1988, in *Physics of formation of Fe II lines outside LTE*, IAU Coll. 94, ed. R. Viotti, A. Vittone, & M. Friedjung, 317
- Sánchez Almeida, J., Asensio Ramos, A., Trujillo Bueno, J., & Cernicharo, J. 2001, *ApJ*, 555, 978
- Schadee, A. 1967, *JQSRT*, 7, 169
- Schüssler, M., Shelyag, S., Berdyugina, S. V., Vögler, A., & Solanki, S. K. 2003, *ApJ*, in press
- Sheeley, N. R. Jr. 1971, *Sol. Phys.*, 20, 19
- Schiavon, R. P., Barbuy, B., & Singh, P. D. 1997, *ApJ*, 484, 499
- Solanki, S. K. 1987, Ph.D. Thesis, ETH, Zürich
- Solanki, S. K., & Bruls, J. H. M. J. 1994, *A&A*, 286, 269
- Solanki, S. K., & Stenflo, J. O. 1986, *A&A*, 170, 120
- Solanki, S. K., Rüedi, I., & Livingston, W. 1992, *A&A*, 263, 312
- Solanki, S. K., Livingston, W., & Ayres, T. 1994, *Sci*, 263, 64
- Sotirovski, P. 1972, *A&AS*, 6, 85
- Steiner, O., Hauschildt, P. H., & Bruls, J. 2001, *A&A*, 372, L13
- Tsuji, T. 1973, *A&A*, 23, 411
- Uitenbroek, H., Noyes, R. W., & Rabin, D. 1994, *ApJ*, 432, L67
- Valenti, J. A., Johns-Krull, C. M., & Piskunov, N. E. 2001, in *The 11th Cambridge Workshop on Cool Stars, Stellar Systems, and the Sun*, ed. R. J. García López, R. Rebolo, & M. R. Zapatero Osorio, San Francisco: ASP Conf. Ser., Vol. 223, CD-1579
- Wallace, L., & Livingston, W. C. 1993, *An Atlas of a Dark Sunspot Umbral Spectrum in the Infrared from 1970 to 8640 cm<sup>-1</sup> (1.16 to 5.1 μm)*, NOAO, Tucson, <ftp://ftp.noao.edu/fts/spot1at1>
- Wallace, L., Hinkle, K., & Livingston, W. C. 2000, *An Atlas of Sunspot Umbral Spectra in the Visible from 15 000 to 25 500 cm<sup>-1</sup> (3920 to 6664 Å)*, NOAO, Tucson, <ftp://ftp.noao.edu/fts/spot4at1>
- Wallace, L., Livingston, W. C., Bernath, P. F., & Ram, R. S. 1998, *An Atlas of the Sunspot Umbral Spectrum in the Red and Infrared from 8900 to 15 050 cm<sup>-1</sup> (6642 to 11 230 Å)*, NOAO, Tucson, <ftp://ftp.noao.edu/fts/spot3at1>
- Wöhl, H. 1971, *Sol. Phys.*, 16, 362